AIAA 2010-982

Modeling the motion of pyrolysis gas through charring ablating material using Discontinuous Galerkin finite elements

Ankush Bhatia[1] and Subrata Roy[2]
Computational Plasma Dynamics Laboratory and Test Facility
Mechanical and Aerospace Engineering Department
University of Florida, Gainesville, FL 32611-6300

A series of efforts were made to solve a simple ablation problem with gas motion through the porous media employing finite element based Galerkin and Discontinuous Galerkin methods. First, one-dimensional solutions of Euler and magneto-hydrodynamics (MHD) equations are presented for comparison with analytical results, to validate the code. The spurious oscillations of standard Galerkin approach were mitigated using Discontinuous Galerkin method. We have shown some preliminary results for the ablation problem using both explicit and implicit Discontinuous Galerkin methods in the paper. However an unresolved exit velocity fluctuations to pressure boundary condition, due to which we are not able to go to target time of 5 seconds for this problem. We plan to resolve these issues, and take this code for application of ablation problems in higher dimensions (2-D or 3-D), and bring in plasma application on the surface.

Nomenclature

B	=	activation energy
C_p	=	specific heat
D	=	diffusion term
e	=	internal energy
E	=	total energy
f	=	friction force per unit volume
K	=	permeability
P	=	pressure
R	=	pyrolysis rate
T	=	temperature
u	=	velocity
ε	=	void fraction
K	=	thermal conductivity
μ	=	viscosity
ρ	=	density
t	=	time

Subscripts

c	=	char
g	=	pyrolysis gas
r	=	resin

I. Introduction

Space vehicles enter earth's (or other planet's) atmosphere while returning from their interplanetary mission. They

[1] Graduate student, Mechanical Engineering Department, University of Florida, student member, AIAA
[2] Associate Professor, Mechanical Engineering Department, University of Florida, Associate Fellow, AIAA

have blunt shaped bodies, which results in high drag force and strong deceleration that help them in landing. Due to high drag, bow shock forms in front of the vehicle, which may be either attached to or detached away from the vehicle's leading surface. This bow shock may interact with viscous boundary layer on the surface, and lead to high viscous dissipation on the surface[1]. This leads to high convection flux on the surface of the vehicle. The gas particles also may get excited into dissociated states which may lead to high radiation flux to the surface. The exact details of this phenomenon are part of hypersonic flow study, with appropriate models for associated chemical reactions. By determining the relevant species, one can apply radiation models, like plane parallel approximation models, to calculate net amount of radiation heat flux to the surface. It has been found that in some cases, radiation heat flux dominates net convective heat flux to the surface[2].

Heat flux to the surface of the vehicle is very high, resulting in temperature rise of several thousand Kelvin. Thermal protective systems (TPS) are used to prevent any damage to the vehicle. These systems are designed to absorb high heat flux, undergo chemical deposition and reject heat load at the surface itself. TPS are characterized into two types, ablative and non-ablative systems[1]. Non-ablating TPS are usually used in reusable hypersonic vehicles, or in cases which do not have very intense entry conditions. Ablative TPS are better, since they allow heat rejection through various mechanisms like phase change, chemical reactions on the surface and inside leading to material removal through gasification. Generation of pyrolysis gas leads to blowing phenomena, which is basically injection of pyrolysis gas into the boundary layer. This helps in achieving convective and radiative blockage[3] reducing the percentage of net heat flux that reaches the surface. The ratio of the TPS material relative to the payload weight plays a critical role in design optimization study which is geared to minimize this ratio[4,5].

Initial efforts of studying ablation began using analytical ablation models, mainly concerned with melting surfaces (ones in which a liquid layer flows over the surface)[6,7]. Later on studies were also applied to direct gasification of solids. Mathematical models were developed based on the understanding of the phenomena, with some simplifying assumptions, like gasification at critical temperature or specifying kinetic mechanism for decomposition process[8]. Second approach allows decomposition over a characteristic range of temperature. But, ablation itself is a complex phenomenon too difficult to be modeled by analytical means. First numerical effort of dealing with ablation was done through development of Charring Material Ablation (CMA) program[9], which treated problem as quasi-one-dimensional, i.e. heat flow was one dimensional, with variable area along the depth. According to [10], CMA considered the steady state flow of pyrolysis gas. Such an assumption may not be a priori evident in steep entry angles conditions, which was the case with Pioneer-Venus Probes[11]. Some studies identify the need for modeling of chemical non-equilibrium of pyrolysis gases in char to correctly simulate their behavior[12,13]. Wakefield and Pitts[14] used CMA to numerically reconstruct thermocouple data for day probe and night probe, and found their temperature values to rise to unrealistically high values for both stagnation point and frustum edge. Governing equations, (1) – (4) were used by to numerically simulate the motion of pyrolysis gas within the char. Interestingly, results obtained in [10] showed closer agreement to flight data. These results were simulated with and without blockage effect and with Wakefield heating rate.

In many of earlier studies, in-depth thermal analyses were done decoupled from hypersonic flow conditions existing outside the vehicle, without any interaction of ablating surface with the flow[15]. Boundary conditions in both the computational fluid dynamics, (CFD) and computational solid mechanics (CSM) were treated in simplified manner, such as constant temperature or heat flux and zero mass transfer. It was suggested in a review paper [15], that coupling both CFD and CSM is essential for an in-depth thermal analysis within the material with appropriate chemical reactions. It was assessed that for such multiphysics problem CFD was formulating non-equilibrium flows, multispecies kinetics, radiation transport etc, but had primitive boundary conditions which prevented their use in TPS design, in a trajectory based analysis. The heat flux at the surface of TPS may be provided as a function of space and time, but still it's a strong function of blowing parameter, which can only be determined through a coupled CFD and CSM analysis along with fully involved surface chemistry. One of the early attempts requiring coupling of both was done in[16], which was to determine the heat shield requirement for Mars Pathfinder, a precursor probe-lander for MESUR mission. It identified the need of specifying empirical blowing parameter in CMA, which will lead to high uncertainties in estimated ablating surface heat flux, and eventually inaccurate temperature histories. Consequently, in [16], Gauss-Seidel implicit aerothermodynamic Navier-Stokes equations with thermochemical surface conditions (GIANTS), and CMA code were used in a loosely coupled manner. Such loosely coupled approach also becomes useful in shape change prediction of a vehicle under ablative conditions. One of the codes, TITAN (Two-dimensional Implicit Thermal Response and Ablation Program), was used along with GIANTS for multidimensional ablation and shape change simulation for graphite sphere-cone TPS[17, 18].

For modeling of chemical reactions in the char material or in gases, there have been several attempts, e.g. ACE[19, 20] (Aerotherm Chemical Equilibrium) code, which solved thermodynamic chemical equilibrium or nonequilibrium kinetics equations between TPS and atmosphere, and then tables were generated which were solved along with fluid dynamics equations. But, ACE did not have good prediction for materials with more than one element with dissimilar ablation

behavior[21]. Consequently a general purpose code, Multicomponent Ablation Thermochemistry was developed in [21]. But, this also generates dimensionless ablation tables. There are many papers that give the details of chemical reactions to consider for a given problem, like Keenan[22], Keenan and Candler[23], Park and Ahn[24] and Suzuki et al.[25].

For more effective designs of future spacecrafts and concepts of aerobraking, it becomes important to accurately model and simulate ablation process. In [26], chemical ablating flows are modeled and relative importance of chemical ablation to thermal ablation is demonstrated. Effect of ionization processes is also shown. There are basically three phenomena by which heat is lost, namely thermal, chemical and mechanical ablation processes. At higher altitudes, where continuum assumption of the working gas breaks down, and rarefied and transition flows are required to model, particle-based DSMC model is used. The modeling effort on ablation is divided into two domains, chemically reacting flows, and thermo-chemically ablating TPS. The work of chemically reacting flows is restricted to either finite volume or finite difference. Our interest is to try and test the capability of finite element methods in this area, since it had already been used to solve for thermally ablating material. We made a series of efforts of solving Euler equations, MHD equations, and then ablation equations with standard Galerkin based Finite element code (details are given below). Due to convergence issues related to Galerkin based FEM; we had to look for methods like Discontinuous Galerkin to solve the current Ablation problem, which considers gas motion inside the ablating material.

Discontinuous Galerkin methods were first applied by Reed and Hill[33] in 1973, to neutron transport problem. They were developed by Cockburn and Shu in a series of papers[34-37], as Total variation diminishing (TVD) Runge Kutta time discretization and DG in space methods to solve nonlinear hyperbolic methods. Discontinuous Galerkin method, in comparison to Galerkin finite element, uses shape functions that are continuous only within the domain of the element and discontinuous across the element's edge. The method uses approximate Riemann solvers (e.g. Godunov or Local Lax-Friedrichs solvers) to evaluate numerical fluxes at to handle discontinuities at cell interfaces. The order of the DG method can be increased by increasing the order of shape function used, and upwind mechanism comes from approximation of inviscid fluxes.

Bassi and Rebay were first to apply Discontinuous Galerkin methods to solving of compressible Navier stokes equations[38]. This was later further developed as Discontinuous Galerkin methods for convection-diffusion problems by Cockburn and Shu[39]. Their method was called 'Local Discontinuous Galerkin' (LDG) methods. Penalty methods developed in 1970s, for purely elliptic problems were brought into unified DG by Arnold et al.[40] For problems with shocks, one needs to either add artificial dissipation to eliminate spurious oscillations, or one needs to use slope limiters to enforce nonlinear stability.

Discontinuous Galerkin method has been applied to different fields like gas dynamics, compressible and incompressible flows, Magnetohydrodynamics, granular flows etc. Their main advantages are high order accuracy, nonlinear stability, and high order parallelizability. In addition they can be used for complex geometries using unstructured meshes, can capture shock without producing spurious oscillations, and are especially built for solving nonlinear hyperbolic problems. We have added a Discontinuous Galerkin module to our in-house code Multi-scale Ionized Gas (MIG) code, and intend to go from current 1-D ablation problem to higher dimensional problems for Ablation. Also, since the code has been tested for flow simulation with DBD plasma actuators in 2-D and 3-D[41, 42], an application of plasma to Ablation is possible in this code, being extensible to higher dimensions.

II. Problem Description

In the present work, we consider the arc-jet problem simulated by Wakefield and Pitts[14], and Ahn and Park[10]. The material in consideration is carbon phenolic, being exposed to 1400 W/cm^2 of heat influx from its right end. The whole problem is considered as 1-D. Thickness of the model is taken to be 1 cm. As the surface on right end ablates due to high temperature rise, resin material pyrolates and decomposes to produce a mixture of gases, denoted as pyrolysis gas. The motion of this gas through the material is not considered in steady state but we solve for the motion of pyrolysis gas through the material, using governing equations (1) – (4).

The produced gas's pressure will increase due to temperature rise and continued pyrolysis, which will result in gas leaking out to atmosphere through the porous material. As a result there will be high velocity (velocity of order of 100 m/s) gas leaking out from the surface, which will provide the essential blockage mechanism to the incoming heat flux, and also help in pushing the shock layer away from the vehicle's surface. The purpose of current work is to study the thermal ablation response of the material for the chosen problem.

III. Governing equations

The ablation problem is considered as one dimensional, and recession is not taken into account at all, for the preliminary efforts. As in [10], temperature of pyrolysis gas is taken to be same as the temperature of solid ablative material. The variables being solved for are, ρ_r, resin density, ρ_g, gas density, u, gas velocity, T, temperature of the solid material, and P, pressure of the pyrolysis gas within the material. 4 governing equations, for ρ_r, ρ_g, u, and T are resin mass, gas mass, gas momentum and overall energy (solid + gas) conservation equations (Equations, 1 – 4)

$$\frac{\partial \rho_r}{\partial t} = -R \tag{1}$$

$$\frac{\partial\left(\varepsilon\rho_g\right)}{\partial t} + \frac{\partial\left(\varepsilon\rho_g u\right)}{\partial x} = R + D \tag{2}$$

$$\frac{\partial\left(\varepsilon\rho_g u\right)}{\partial t} + \frac{\partial\left(\varepsilon\rho_g u^2 + \varepsilon P\right)}{\partial x} = -\varepsilon f + I \tag{3}$$

$$-\frac{\partial}{\partial t}\left(\rho_c e_c + \rho_r e_r + \varepsilon\rho_g e_g + \frac{1}{2}\varepsilon\rho_g u^2\right) + \frac{\partial}{\partial x}\left[\varepsilon u\left(\rho_g e_g + \frac{1}{2}\rho_g u^2 + P\right)\right] = \frac{\partial}{\partial x}\left(k\frac{\partial T}{\partial x}\right) \tag{4}$$

Here ε represents void fraction in the ablative material, and is given by (5), where ρ_p specifies intrinsic density of resin, which is equal to 1763.6 kg/m^3. Source terms in above equations, namely R, D, f, and I stand respectively for pyrolysis rate due to decomposition of the material, diffusion that expresses rate of change of pyrolysis gas density due to spatial varying pressure, derived from negative of divergence of flux given by Darcy's law [10], friction to the flow due to porosity of the medium (less porosity, i.e. low ε, will mean high frictional resistance on the gas flow) and Inertial force that accounts for deviation from Darcy's law, when velocity of diffusing gas is high. These source terms are given in equations (6) – (9), as reported in [10].

$$\varepsilon = \varepsilon_{\max} - \rho_r / \rho_p \tag{5}$$

$$R = \sum_{k=1}^{N} A_k \exp\left(-\frac{B_k}{T}\right)\rho_v\left(\frac{\rho_r}{\rho_v}\right)^n \tag{6}$$

$$D = \frac{K}{\mu}\left(\varepsilon\rho_g\right)\varepsilon\frac{\partial^2 P}{\partial x^2} \tag{7}$$

$$f = \left(\frac{\mu}{k}\right)u \tag{8}$$

$$I = 1.222\left(\frac{1}{\sqrt{k}}\right)\rho_g u^2 \tag{9}$$

In (5) – (9), K and μ stand for gas permeability and viscosity, and their expressions and for all other variables in (5) – (9) are given in [10], and reader is referred to this paper for further formulation details. Ref. [10] gives values for k, thermal conductivity of carbon-phenolic material and Cp_C, specific heat of solid carbon char as a function of Temperature, but value of Cp_r was not reported, which was taken to be a constant value of 1174 W/m.K for this work. Pyrolysis Gas is a species of 14 gas components, C, CH, CH_2, CH_3, CH_4, CO, CO_2, C_2, C_3, H, HO, H_2O, O, and O_2 taken to be at equilibrium at the temperature of the solid material. Pressure of the gas was obtained through use of chemical solver, CANTERA[27], in which initial composition were given as, C: 1.3527, H: 6.4557, O: 1, being composition of resin. The input to CANTERA for all thermodynamic calculations is through a CTI file, and properties like specific heat, enthalpy, and entropy are specified as functions of temperature, in terms of NASA polynomials, for

each of the components of the pyrolysis gas. For non-equilibrium analyses, reactions and their rates (in Arrhenius coefficients) can also be specified in this CTI file. The equilibrium properties like internal energy, pressure, enthalpy, temperature etc. can be found by specifying initial composition (by mol fraction) of the mixture, and equilibrium criteria at constant temperature and pressure.

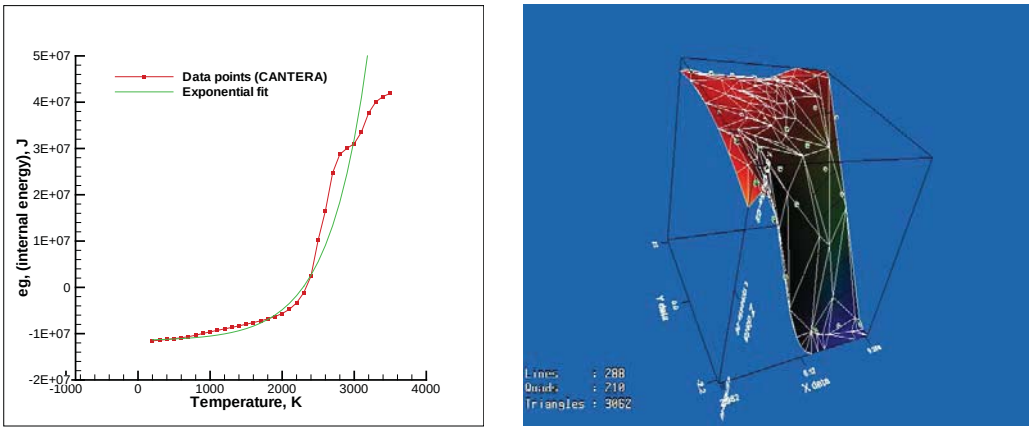

Figure 1: Above Plot shows variation of internal energy (J/kg) of pyrolysis gas with Temperature of the gas (in K). Line in red, with red dots shows data collected from CANTERA, and line in green shows exponential fit evaluated using TECPLOT. As we see above, the fit is useful only up to temperature of nearly 3000 K.

Thus, we got e_g, internal energy of gas and MW, the molecular weight of the gas for different Temperature and density of gas. The data points for both, e_g and MW were exponentially fitted to get a plot that grows monotonically, and to avoid any discontinuity in the gradients of these properties. The expression of e_g, was obtained using TECPLOT, while 3D data for MW (in terms of temperature and density) was curve fitted using an online software, ZunZun.com[28]. Their expressions are given below. We used second order polynomial in logarithm (of base 10) in density and fourth order polynomial in Temperature. X-axis is from 2.952 to 9.288, which stands for Temperature, Y-axis is from -2.2 to 2.2, which stands for $\text{Log}_{10}(\rho_g)$ and Z – axis is from 4.872e-3 to 1.8317e-2, which is for Molecular weight of gas in Kg/mol. The plot of the curve fitted can be seen in figure 2, which was plotted using VRMLview[32]. CANTERA is seen as a potential source for future for including effects of chemical reactions in the flow solver. It will be compared in coming future, for its performance, ease of implementation and solution accuracy compared to current ways of solving chemically reacting flows and results.

$$e_g = \exp\left(A_1 T + A_2\right) - A_3 \tag{10}$$

$$MW = B_1 \exp\left(y\right) + B_2 \exp\left(x\right) + B_3 \exp\left(x\right)\exp\left(y\right) + B_4 \tag{11}$$

Where, the constants for equation (10), are given as A_1 = 1.869e-03, A_2 = 1.198exp+01 and A_3 = 1.156exp+07. For equation (11), x and y depend on temperature and gas density respectively as, x = $(T/1000)^2$ and y = $\text{LOG}_{10}(\rho_g)$, and constants are given by, B_1 = 1.7981exp-04, B_2 = -1.333exp-06, B_3 = 2.0159exp-07, and B_4 = 1.678exp-02. Prior to above exponential fits, polynomials curves were fitted through the data, and it was found that the resulting plots had non-monotonic behavior, which can cause issues in simulation, like pressure gradient might shift signs from positive to negative, and that can affect solution accuracy.

IV. Numerical Scheme

A. Galerkin Finite Element Method with Sub-Grid Embedding scheme

Our In-house Multi-scale Ionized Gas flow code; MIG was used to solve the ablation problem. The discretization scheme employed in the code is Standard Galerkin based Finite element. Local element stiffness matrices are built in the 'element_library' subroutine, which are assembled into global matrix. For time stepping, we use θ-implicit approach, and

for fully implicit time integration, we use θ = 1.0. Newton Raphson scheme is used for solving highly non-linear problems. The assembled global matrix is solved using generalized minimal residual method, GMRES, an iterative way for solving a system of linear equations. The governing equations, are converted from conservative to a non-conservative form, and then integrated with the basis function to obtain the discretized weak form. A simple example of burger's equation with a given source term, is shown just to demonstrate the discritizing process.

$$\frac{\partial U}{\partial t}+\frac{1}{2}\frac{\partial\left(U^2\right)}{\partial x}=0 \qquad \longrightarrow \qquad \frac{\partial U}{\partial t}+U\frac{\partial U}{\partial x}=0$$

(Conservative form) (Non-conservative form)

$$\int\{V\}\left(\frac{\partial\{U\}}{\partial t}+\{U\}\frac{\partial\{U\}}{\partial x}\right)dx=\int\{V\}.\{G\}dx \tag{12}$$

Both, U and V are approximated by U_h and V_h, and then written in terms of their nodal values and Lagrange shape functions (denoted by N),

$$U_h=\{N\}^T\{U_j\} \tag{13}$$

$$V_h=\{N\}^T\{V_j\} \tag{14}$$

Final weak form for the equations is given by,

$$\int\{N\}\{N\}^T\left(\frac{\{U_j\}^{n+1}-\{U_j\}^n}{\Delta t}\right)dx+\int\{N\}\{U\}\left\{\frac{DN}{DX}\right\}^T\{U_j\}^{n+1}dx=\int\{N\}.\{G\}^{n+1}dx \tag{15}$$

Where, $\{N\}\{N\}^T$ denotes mass matrix, and $\{N\}\{U\}\{DN/Dx\}^T$ is hyper matrix, where U is just evaluated at the required location in the integration. If {G} depends on {U}, then the expression is placed into element stiffness matrix, by using Newton's method, else it just sits as a source vector on right hand.

Successful solving of Euler equations and MHD equations using Galerkin Finite element, requires use of artificial dissipation. Sub-Grid Embedding (SGM) developed by Roy et al.[29] was employed as an artificial dissipation mechanism, which enabled successful solution of both the equations.

Ablation problem was also solved with MIG code, but it results in oscillations in the solution, as discussed in results section. Since paper [10], uses a loosely coupled formulation for solving equations (1), (4) and (2), (3) as two separate sets, we also implemented this into our system, to see if it resulted in any improvement for solution. This however didn't help in getting rid of oscillations.

Seeing inevitable oscillations in the solution, and incapability of SGM, artificial dissipation scheme, to overcome these oscillations, we decided for implementing upwind based finite element procedures into our framework, and Discontinuous Galerkin scheme seemed to have most attractive features, due to its high order accuracy, simple implementation, and easy extension to higher dimensions, which seemed promising for our future goals to extend the Ablation problem to 3-D. We built 3 codes for Discontinuous Galerkin method.

1) Explicit Runge Kutta Discontinuous Galerkin method
2) Explicit Discontinuous Galerkin module in MIG
3) Implicit Discontinuous Galerkin module in MIG

B. Explicit Runge Kutta Discontinuous Galerkin method

Explicit Runge Kutta Discontinuous Galerkin Method was developed by Cockburn and Shu in their series of papers, [34] – [37] and some sample problems as mentioned in [43], like Advection equation, Burger equation, and heat

conduction problem were tested using this code. The basic DG formulation is given as follows. By use of Legendre polynomials as basis function, we are able to decouple the resulting system of equations into totally explicit equations, by which we can solve equations node by node. This makes the system suitable for parallelization, an advantage that offsets the increased degree of freedoms in DG method. For time integration for resulting ODE's, we use a 3rd order Runge Kutta time integration scheme.

$$\frac{\partial U}{\partial t}+\frac{\partial F(U)}{\partial x}+\frac{\partial F_v(U,\nabla U)}{\partial x}=G(U) \tag{16}$$

U represents vector of solution variable that we are interested in solving for. F and F_v are Inviscid and viscous flux vectors and G is the source vector. Above system of equations are multiplied by arbitrary smooth functions, V and then integrated over an element, with interval $I_j \equiv \left(x_{j-1/2}, x_{j+1/2}\right)$. Integration by parts to the resulting system of equations and approximating U by U_h and V by V_h, leads to following system of equations,

$$\begin{aligned}&\int_{I_j}\frac{\partial}{\partial t}U_h(x,t)V_h(x)\,dx-\int_{I_j}F\left(U_h(x,t)\right)\frac{\partial}{\partial x}V_h(x)\,dx+H\left(U_h\right)_{j+1/2}(t)V_h\left(x_{j+1/2}^-\right)\\&-H\left(U_h\right)_{j-1/2}(t)V_h\left(x_{j-1/2}^+\right)-\int_{I_j}F_v\left(U_h(x,t),S_h\right)\frac{\partial}{\partial x}V_h(x)\,dx+H_v\left(U_h,S_h\right)_{j+1/2}(t)V_h\left(x_{j+1/2}^-\right)\\&-H_v\left(U_h,S_h\right)_{j-1/2}(t)V_h\left(x_{j-1/2}^+\right)-\int_{I_j}G\left(U_h(x,t)\right)V_h(x)\,dx=0\end{aligned} \tag{17}$$

U_h and V_h are written in terms of basis function (Legendre polynomials are used here) , and we obtain following system of equations,

$$U_h=\sum_{l=0}^{k}U_j^l\phi_l(x) \tag{18}$$

$$\phi_l(x)=P_l\left(2\left(x-x_j\right)/\Delta_j\right) \tag{19}$$

$$\begin{aligned}&\left(\frac{1}{2l+1}\right)\frac{\partial}{\partial t}U_j^l(t)-\frac{1}{\Delta_j}\int_{I_j}F\left(U_h(x,t)\right)\frac{\partial}{\partial x}\phi_l(x)\,dx-\frac{1}{\Delta_j}\int_{I_j}F_v\left(U_h(x,t),S_h(x,t)\right)\frac{\partial}{\partial x}\phi_l(x)\,dx\\&-\frac{1}{\Delta_j}\int_{I_j}G\left(U_h(x,t)\right)\phi_l(x)\,dx+\frac{1}{\Delta_j}\left\{H\left(U_h\left(x_{j+1/2}\right)\right)(t)-(-1)^l H\left(U_h\left(x_{j-1/2}\right)\right)(t)\right\}\\&+\frac{1}{\Delta_j}\left\{H_v\left(U_h\left(x_{j+1/2}\right),S_h\left(x_{j+1/2}\right)\right)(t)-(-1)^l H_v\left(U_h\left(x_{j-1/2}\right),S_h\left(x_{j+1/2}\right)\right)(t)\right\}=0\end{aligned} \tag{20}$$

Δ_j is the length of interval I_j. An auxiliary variable, S is introduced to replace ∇U, with an additional auxiliary equation for S. For more details on how to apply DG for viscous fluxes, please refer to [43]. H and H_v are numerical fluxes that depend on solution variable on both sides of the node in the subscript. For Inviscid fluxes, both Godunov flux, and Local Lax-Friedrichs flux have been used. Godunov flux is well-known due to its smallest amount of artificial viscosity that is introduced into the scheme. Local lax Friedrichs produces more artificial viscosity than Godunov flux, and is suitable when f is complicated, as in our case. For viscous fluxes, BR-1 scheme is used, which is simple averaging of flux values from both sides of the node, ($x_{j-1/2}$ or $x_{j+1/2}$).

$$H^G(a,b)=\begin{cases}\min_{a\le u\le b} F(u), if\ (a\le b)\\ \max_{a\le u\le b} F(u), otherwise\end{cases} \tag{21}$$

$$H^{LLF}(a,b)=\frac{1}{2}\left(F(a)+F(b)-\alpha(b-a)\right)$$
$$\alpha=\max_{\min(a,b)\le s\le\max(a,b)}\left|\frac{\partial F}{\partial U}(s)\right| \tag{22}$$

$$H_v(a,b)=\frac{1}{2}\left(F_v(a)+F_v(b)\right) \tag{23}$$

Resulting system of equations, are ODEs which are integrated in time, using Runge Kutta time discretization method. We have used 3rd order Runge Kutta time discretization for this part. Please refer to [43] for details on Runge Kutta time discretization.

C. Explicit Discontinuous Galerkin Module in MIG

Being limited by very small time step for Explicit Runge Kutta Discontinuous Galerkin method, we decided on implementing Implicit Discontinuous Galerkin scheme into MIG as a separate module. This formulation requires use of matrices, and due to inbuilt structure of implicit solver in MIG, it seemed lucrative and time efficient to use the framework built in MIG. Since MIG has been implemented for 2-D and 3-D problems in plasma, this module can also be easily extended to higher dimensions. As a first step therefore, Explicit Discontinuous Galerkin method using matrix system (rather than decoupled equations in Explicit RKDG above) was implemented to check its working with already developed and fully tested Runge Kutta Explicit DG code. The formulation for Explicit DG code, as different from Explicit RKDG, is as follows.

$$\left[\int\{\phi\}\{\phi\}^T dx\right]\frac{\partial\{U_j^l\}}{\partial t}-\int\left\{\frac{\partial\phi}{\partial x}F\right\}dx+|\,\phi.F\,|_-^+-\int\left\{\frac{\partial\phi}{\partial x}F_v\right\}dx+|\,\phi.F_v\,|_-^+=\int\{\phi G\}\,dx \tag{24}$$

The term in square brackets (with unsteady term) is a diagonal mass matrix since the basis functions are Legendre polynomials. Applying forward Euler time integration for unsteady terms, we get final form of system of equations to be solved.

$$[M]\left[\frac{\{U_j^l\}^{n+1}-\{U_j^l\}^n}{\Delta t}\right]=\int\left\{\frac{\partial\phi}{\partial x}F\right\}dx-|\,\phi.F\,|_-^++\int\left\{\frac{\partial\phi}{\partial x}.F_v\right\}dx-|\,\phi.F_v\,|_-^++\int\{\phi.G\}\,dx \tag{25}$$

M denotes mass matrix, and right hand side above is known at previous time step. Note for auxiliary equations the term in bracket with [M], will change to simply $\{U_j^l\}^{n+1}$.

Here also, both Godunov and Local Lax-Friedrichs flux was used for approximation of numerical fluxes of Inviscid flux vector, F. For LLF, α is maximum eigenvalue of Jacobian matrix $\frac{\partial F}{\partial U}$. For Euler and Ablation equations, Jacobian matrix and eigenvalues are given below.

Euler equations

$$\frac{\partial F}{\partial U}=\begin{bmatrix} 0 & 1 & 0 \\ -\frac{(3-\gamma)}{2}u^2 & (3-\gamma)u & \gamma-1 \\ (\gamma-1)u^3-\gamma uE & \gamma E-\frac{3}{2}(\gamma-1)u^2 & \gamma u \end{bmatrix} \tag{26}$$

$$\lambda_{1,2,3}=u,u-c,u+c \tag{27}$$

γ is ratio of specific heats, and c is the speed of sound.

Ablation equations

$$\frac{\partial F}{\partial U}=\begin{bmatrix} 0 & 0 & 0 & 0 & 0 & 0 \\ 0 & 0 & 1 & 0 & 0 & 0 \\ A & B & D & F & 0 & 0 \\ u*A & C & E & u*F & 0 & 0 \\ 0 & 0 & 0 & 0 & 0 & 0 \\ 0 & 0 & 0 & 0 & 0 & 0 \end{bmatrix} \tag{28}$$

Expressions for A, B, C, D, E, F is given in appendix.

$$\lambda_{1,2,3}=0,u\pm\frac{\left(\begin{array}{l}\rho_g{}^2\varepsilon\frac{\mathrm{de_g}}{dT}P\left(\rho_rC_{pr}+\rho_cC_{pc}\right)+\rho_g\rho_r{}^2C_{pr}^2P \\ +\rho_g\rho_c{}^2C_{pc}^2P+2\rho_g\rho_rC_{pr}P\rho_cC_{pc}\end{array}\right)^{\frac{1}{2}}}{\rho_g\left(\rho_rC_{pr}+\rho_cC_{pc}+\varepsilon\rho_g*\frac{\mathrm{de_g}}{dT}\right)}=0,u\pm c_{\mathrm{mod}} \tag{29}$$

c_{mod} is denoted as modified speed of sound, since the structure of eigenvalues resembles that of Euler equations.

D. Implicit Discontinuous Galerkin Module in MIG

Formulation for Implicit DG, will be same as (), but the right hand side now is dependent on solution vector, U and at current time step. Since RHS is also unknown, this is a linear problem and requires use of Newton's method to solve system of equations. For Newton's method, we require evaluation of Jacobian, i.e. derivates of Inviscid flux, viscous flux and source vectors need to be computed. Resulting Jacobian for system of equations (), is thus given as,

$$J\equiv M-\Delta t\left(\int\frac{\partial\phi}{\partial x}.\frac{\partial F}{\partial U}dx-\left[\phi^+.\frac{\partial F^+}{\partial U}-\phi^-.\frac{\partial F^-}{\partial U}\right]+\int\frac{\partial\phi}{\partial x}.\frac{\partial F_v}{\partial U}dx-\left[\phi^+.\frac{\partial F_v{}^+}{\partial U}-\phi^-.\frac{\partial F_v{}^-}{\partial U}\right]+\int\phi.\frac{\partial S}{\partial U}dx\right) \tag{30}$$

The derivatives for F, F_v, and G are given below for Ablation equations. F^+ and F^- depend on U from element at j and the neighboring element (j+1 or j-1), hence their derivatives w.r.t. U_j and U_{j+1} or U_{j-1} (depending on if we have F^+ or F^-) need to be evaluated and placed accordingly in the global matrix assembly. For implementation, of Implicit Discontinuous Galerkin to MIG, for both Euler equations, and Ablation equations, only Local Lax-Friedrichs flux was found to work. We found that Jacobian of Godunov flux didn't satisfy linearization check, as explained in appendix.

$$\frac{\partial F_v}{\partial U} = \begin{bmatrix} 0 & 0 & 0 & 0 & 0 & 0 \\ 0 & -\frac{K_g}{\mu}\varepsilon S_1 & 0 & 0 & -\frac{K_g}{\mu}(\varepsilon\rho_g)\varepsilon & 0 \\ 0 & 0 & 0 & 0 & 0 & 0 \\ 0 & 0 & 0 & 0 & 0 & -k_{cond} \\ -\frac{\partial P}{\partial \rho_r} & -\frac{\partial P}{\partial \varepsilon\rho_g} & -\frac{\partial P}{\partial \varepsilon\rho_g u} & -\frac{\partial P}{\partial E} & 0 & 0 \\ -\frac{\partial T}{\partial \rho_r} & -\frac{\partial T}{\partial \varepsilon\rho_g} & -\frac{\partial T}{\partial \varepsilon\rho_g u} & -\frac{\partial T}{\partial E} & 0 & 0 \end{bmatrix} \tag{31}$$

$$\frac{\partial S}{\partial U} \equiv \begin{bmatrix} -2R/\rho_r & 0 & 0 & 0 & 0 & 0 \\ 2R/\rho_r & 0 & 0 & 0 & 0 & 0 \\ 0 & -\frac{(-\varepsilon f + I)}{\varepsilon\rho_g} & \left(-\frac{\mu}{K_g\rho_g} - \frac{2.444|u|}{\varepsilon\sqrt{K_g}}\right) & 0 & 0 & 0 \\ 0 & 0 & 0 & 0 & 0 & 0 \\ 0 & 0 & 0 & 0 & 0 & 0 \\ 0 & 0 & 0 & 0 & 0 & 0 \end{bmatrix} \tag{32}$$

Implicit method requires rigorous check of the linearization of jacobians, and jacobians need to be modified for F^+ and F^- at the boundary nodes. Same has to be done for viscous flux vectors. Derivatives for F^+ and F^- in general for interior nodes is given as,

$$\frac{\partial F^+}{\partial U} = \frac{1}{2}\left(\left.\frac{\partial F}{\partial U}\right|_{U=U^-} + \alpha(u)\delta_{ij} - \left(\alpha'_{U^-}(U)\right)_j \left(U^+ - U^-\right)_i \right) \tag{33}$$

$$\frac{\partial F^-}{\partial U} = \frac{1}{2}\left(\left.\frac{\partial F}{\partial U}\right|_{U=U^+} - \alpha(u)\delta_{ij} - \left(\alpha'_{U^+}(U)\right)_j \left(U^+ - U^-\right)_i \right) \tag{34}$$

if U belongs to element at j, and since F^+ and F^- also depend on U from adjacent element, their derivatives w.r.t. U needs to be placed in the same row for element at j, but columns for elements at j+1 or j-1, whichever is applicable. Derivatives of F^+ and F^- w.r.t. U from neighboring elements is given as,

$$\frac{\partial F^+}{\partial U} = \frac{1}{2}\left(\left.\frac{\partial F}{\partial U}\right|_{U=U^+} - \alpha(u)\delta_{ij} - \left(\alpha'_{U^+}(U)\right)_j \left(U^+ - U^-\right)_i \right) \tag{35}$$

for U belonging to element on right, and,

$$\frac{\partial F^{-}}{\partial U}=\frac{1}{2}\left(\left.\frac{\partial F}{\partial U}\right|_{U=U^{-}}+\alpha(u)\delta_{ij}-\left(\alpha'_{U^{-}}(U)\right)_{j}\left(U^{+}-U^{-}\right)_{i}\right) \tag{36}$$

for U belonging to element on left

α is maximum eigenvalue given in equation (29), therefore its derivative w.r.t. U is,

$$\frac{\partial\alpha}{\partial(\varepsilon\rho_g)}=-\frac{u}{\varepsilon\rho_g}\pm c_{\text{mod}}\left[\begin{array}{l}-\dfrac{\left(e_g+\dfrac{u^2}{2}\right)}{2\left(P\left(Cp_r\rho_r+Cp_c\rho_c\right)\right)}+\dfrac{1}{2}\dfrac{\left(2\rho_g\dfrac{\mathrm{de_g}}{dT}+\dfrac{1}{\varepsilon}\left(Cp_r\rho_r+Cp_c\rho_c\right)\right)}{\left(\rho_g^2\varepsilon\deg+\rho_g\left(Cp_r\rho_r+Cp_c\rho_c\right)\right)}\\ -\dfrac{1}{\varepsilon\rho_g}-\dfrac{\dfrac{\mathrm{de_g}}{dT}}{\left(Cp_r\rho_r+Cp_c\rho_c+\varepsilon\rho_g\dfrac{\mathrm{de_g}}{dT}\right)}\end{array}\right] \tag{37}$$

$$\frac{\partial\alpha}{\partial(\varepsilon\rho_g u)}=-\left[-\frac{1}{\varepsilon\rho_g}\pm\frac{u.c_{\text{mod}}}{2\left[E-\varepsilon\rho_g e_g-\dfrac{1}{2}\varepsilon\rho_g u^2-\rho_r h_r^0\right]}\right] \tag{38}$$

$$\frac{\partial\alpha}{\partial E}=\pm\frac{c_{\text{mod}}}{2\left[E-\varepsilon\rho_g e_g-\dfrac{1}{2}\varepsilon\rho_g u^2-\rho_r h_r^0\right]} \tag{39}$$

Positive and minus signs in above expressions are selected based on whether maximum eigenvalue chosen in (29) is $(u + c_{mod})$ or $(u - c_{mod})$.

V. Boundary & Initial Conditions

Total grid size is taken to be 1 cm, and the inner boundary is fixed at x = 0 cm and outer boundary at x = 1 cm. Boundary conditions are as follows. No boundary conditions are needed for equation (1), since it's a pure unsteady differential equation. For (2), ρ_g no boundary conditions are specified at x = 0 cm. At x = 1 cm, ρ_g is found by solving the state equation, i.e. MW as a function of ρ_g and T, which basically relates Pressure, gas density and Temperature. Pressure at x = 1 cm, is given to be 0.22 atm (Arc jet test data in [10]), and Temperature will be known by solid's temperature. For (3), u is taken to be 0 m/s and adiabatic boundary condition for Temperature (equation (4)) at x = 0 cm.

At x = 1.0 cm, equation (1), as mentioned, doesn't need a boundary condition, (2)'s boundary condition has already been specified above. No boundary condition is applied on velocity at x = 1 cm. For temperature, an incoming heat flux (in negative X direction) of 1400 W/cm^2 is specified. Initial conditions are uniform throughout the domain for all 4 variables; ρ_r is 250 kg/m^3, ρ_g is 6.05e-3 kg/m^3 (evaluated @ P = 0.22 atm, and T = 300.0 K), u is 0 m/s and T is 300.0 K.

V. Results and Discussions

Since Gas equations in equations (1) – (4), are similar in form to Euler equations, an initial test for the MIG code was done for 1-D Euler equations, and 1-D MHD equations. Subsequently for development of Discontinuous Galerkin scheme, Euler equations were used as test problems to check working of the DG code. The results are shown below. Sub-grid embedding (SGM)[29] was used to control the oscillations in the solution that generally appear with a convection term in the Galerkin framework.

A. Euler equations and MHD equations with Galerkin FEM

First problem tried on MIG, is Sod's Shock tube case[30]. The domain is from x = 0 m to 1 m, and boundary conditions are ρ = 1.0 kg/m3, u = 0.0 m/s, P = 1.0 Pa at x = 0 m, and ρ = 0.125 kg/m3, u = 0.0 m/s, P = 0.1 Pa at x = 1 m. Initial solution was a sharp discontinuity in both Pressure and density profiles with discontinuity at x = 0.5 m. The solution was solved with SGM, an artificial diffusion approach that minimizes all oscillations, which can propagate in the solution domain and destroy the solution. The results are compared with exact solution available in any standard textbook on numerical computations of fluid flows, like [30]. The solution was run with Δt = 1.0e-4 sec up till t = 0.2 sec, and the results are shown for both 1001 and 101 nodes in figures 2 and 3 respectively. The initial discontinuity basically represents state of perfect gas, in shock tube, where a diaphragm in center separates gas in both chambers (left and right) at two different conditions. At t = 0 sec, this chamber is broken, and this leads to travelling shock in the right chamber, and travelling expansion wave in the left chamber. The travelling shock is accompanied by a contact discontinuity, which moves at lower speed to the right chamber.

With 1001 nodes for shock tube problem, we got close results with SGM. Shock's position in numerical solution came out to be 0.837 m, as compared to 0.8501 m for exact solution. Density, left to contact discontinuity, is 0.42568 kg/m3 (numerical) and that to left of shock is 0.26524 kg/m3. The exact values at these locations respectively are 0.42 kg/m3 and 0.26 kg/m3 (Get exact values at this location). Velocity is very close to exact value of 0.92 m/s. Pressure ratio across the shock is obtained as 3.084, as compared to exact value of 3.025. When the solution was run with 101 nodes, we noticed that curbing of oscillations by use of SGM, was more difficult, but still the solution was close to the exact as shown in figures. It is easier to curb out high frequency oscillations with selective diffusion scheme, than to curb out lower frequency oscillations. Higher diffusion to curb out oscillations near discontinuity will result in smearing of the shock profile more across mesh elements. The effect of SGM on oscillations can be seen in figure 4, which are shown for a 100 nodes mesh, where solution for ρ and u shows exact solution, and numerical result with and without SGM. We can clearly see the dissipation of the oscillations, without much smearing of the solution in the whole domain.

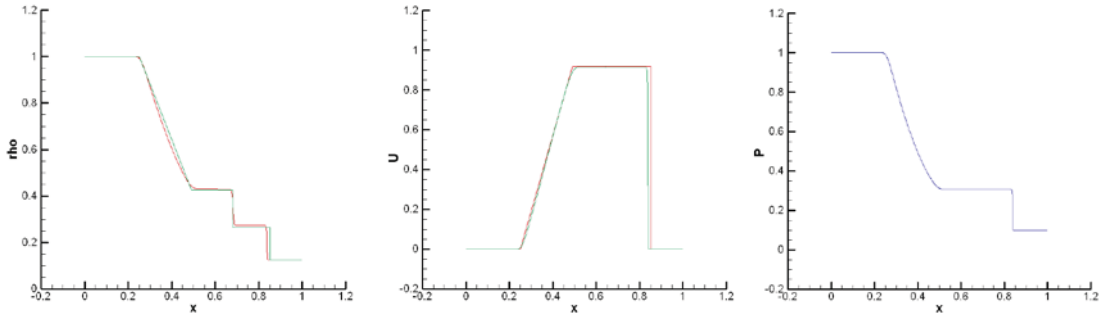

Fig. 2: Comparison of numerically obtained results ρ, u, P, with exact solutions for 1001 nodes in mesh. SGM was employed for selective artificial diffusion. Red color for ρ, u indicates exact solution and green color indicates numerical solution. Pressure was compared by shock's location and ratio of pressure on to left of shock to its right end.

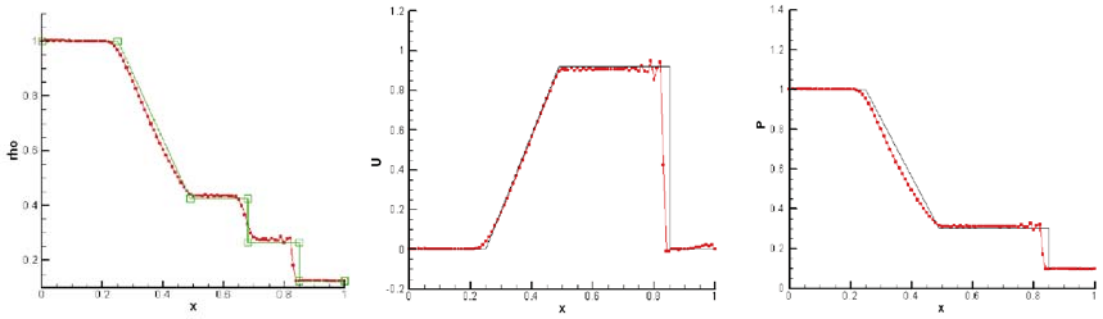

Fig. 3: Comparison of numerically obtained results ρ, u, P, with exact solutions for 101 nodes in mesh. SGM was employed for selective artificial diffusion. Red color indicates numerical solution and other color indicates exact solution.

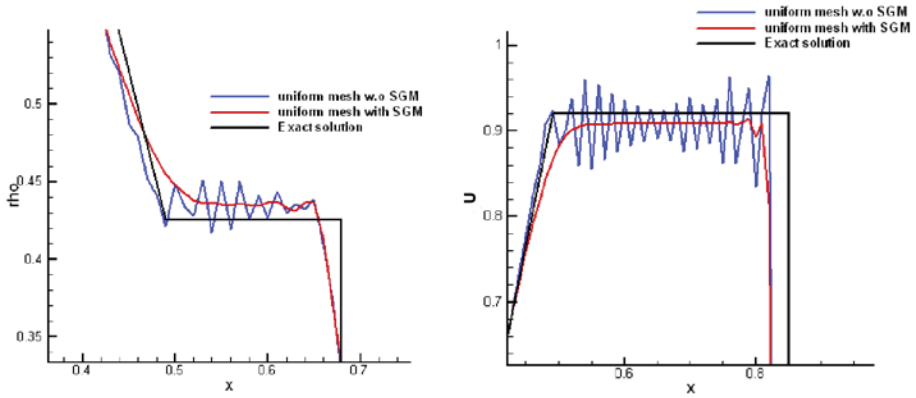

Fig. 4: Blue color indicates solution without SGM, and red with SGM. Black color indicates exact solution. We see the effect of SGM in reducing oscillations without much of smearing of the solution.

Second problem solved by MIG was 1-D MHD compound shock-wave problem. MHD equations are fluid dynamics equations coupled with Maxwell's electrodynamics equations, which describe the flow of conducting fluid in a magnetic field[31]. By making some assumptions, like neglecting displacement current, viscosity, resistivity etc. we get "ideal" MHD equations. A simplified 1-D form of MHD equations is given below along with the boundary conditions. The results are also shown, both with and without SGM in figure 5. Again we see the effect of SGM in curbing all oscillations, without smearing or destroying of the overall solution. γ for this problem was chosen to be 2, to compare the results with [31]. The given system of MHD equations is non-convex as well as not-strictly hyperbolic for reasons described in [31]. The domain size is from x = 0 m to x = 800 m, Δx = 1 m, and Δt = 0.2 sec, and solution is ran up till 80 sec of total time. Initial solution has discontinuity in Density, Magnetic field in y-direction, and Pressure at x = 400 m. Magnetic field in x-direction is held constant at a value of 2.66 T. The solution of MHD equations shows fast rarefaction wave moving to the left, and a slow compound wave next to it. The waves moving to right are contact discontinuity in middle, slow shock wave next to it and fast rarefaction to the extreme right.

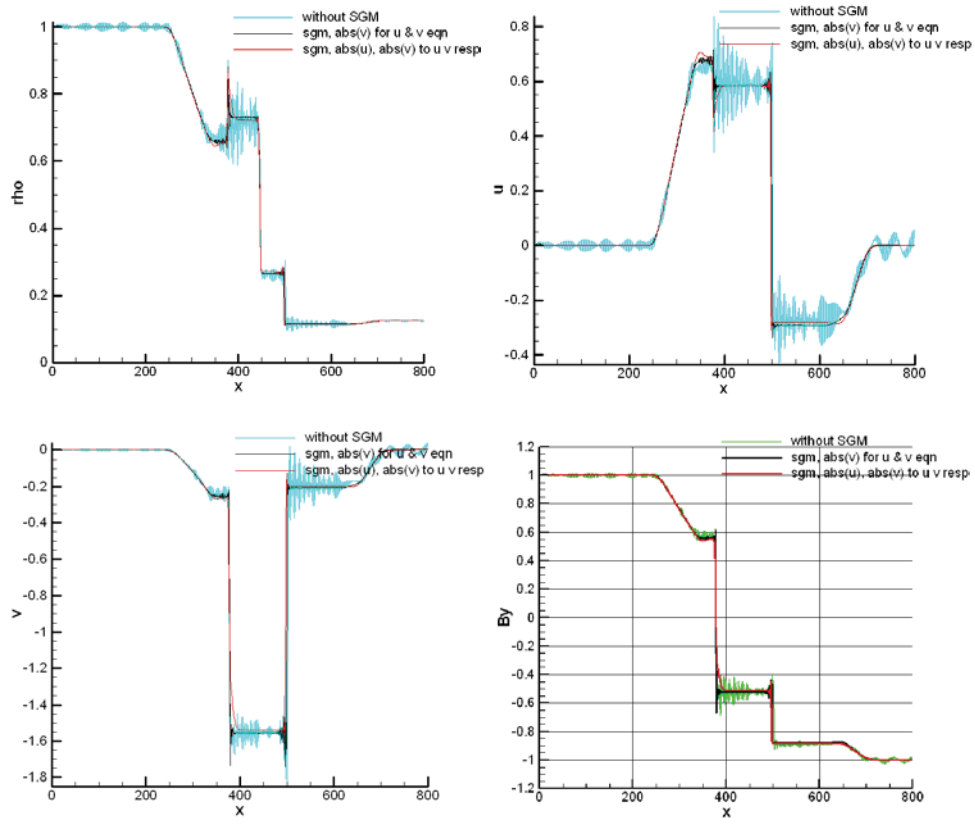

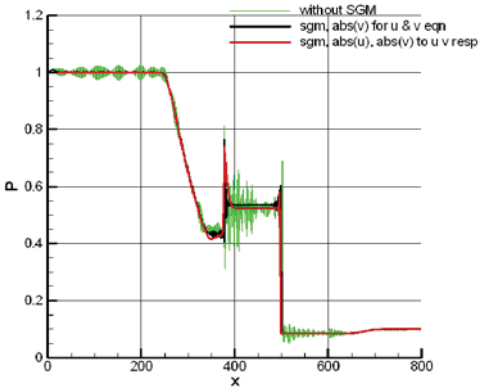

Fig. 5 : Results obtained with MIG Code for 1-D MHD Problem for ρ, u, v, By, P. Plots show again comparison between solutions without SGM and with SGM for u and v equations, in two forms for the factor used. The above solution shows close resemblance to exact solution.

$$\frac{\partial \rho}{\partial t} + u\frac{\partial \rho}{\partial x} + \rho\frac{\partial u}{\partial x} = 0$$

$$\frac{\partial u}{\partial t} + u\frac{\partial u}{\partial x} + \frac{1}{\rho}\frac{\partial P}{\partial x} + \frac{B_y}{\rho}\frac{\partial B_y}{\partial x} = 0$$

$$\frac{\partial v}{\partial t} + u\frac{\partial v}{\partial x} - \frac{B_x}{\rho}\frac{\partial B_y}{\partial x} = 0$$

$$\frac{\partial B_y}{\partial t} + B_y\frac{\partial u}{\partial x} + u\frac{\partial B_y}{\partial x} - B_x\frac{\partial v}{\partial x} = 0$$

$$\frac{\partial P}{\partial t} + 2P\frac{\partial u}{\partial x} + u\frac{\partial P}{\partial x} = 0$$

BOUNDARY CONDITIONS:

ρ= 1.0 @ Left, ρ = 0.125 @ Right

u, v = 0.0 @ Both ends

By = 1.0 @ Left, By = -1.0 @ Right

P = 1.0 @ Left, P = 0.1 @ Right

(40)

B. Ablation problem with Galerkin FEM

After above two attempts at solving Shock tube problem and MHD compound shock problem, ablation problem was attempted in its entirety. But, due to difficulty in convergence, some simplifications were attempted to observe the effect of simplifications on our ability to solve the ablation problem. What follows is a series of efforts to simplify the ablation problem, and obtained results are reported with standard Galerkin approach.

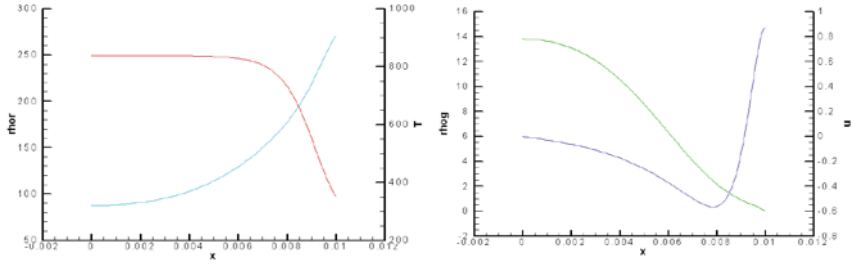

Fig. 6 : Solution of Ablation equations some simplifications, like neglecting terms like D and I, and taking constant value of e_g and e_r.

First attempt was to treat some of the terms appearing in the equations as constant. For example, first case was eliminating D and I from equations (2) and (3). These are basically driving terms for gas flow, apart from Pressure gradient in equation (3). With constant values of e_g and e_r at 1.141e07 J/kg and 2.20e06 J/kg. The solution was run for total time of 1 sec, and obtained results are shown in figure 6. This shows a negative velocity profile. The velocity is

mainly driven by Pressure gradient (only being restrained by friction), which depends on the gradients of both Temperature and gas density. So, Pressure gradient being dependent on T and ρ_g, has a maxima in the solution domain and hence drives the gas in two directions, as seen in the solution. General shape of Temperature, resin density and gas density make sense, since Heat flux from right hand side, leads to increase in temperature on right end, and then through heat conduction, there's a resultant rise in temperature inside the material, which leads to pyrolysis in that zone, due to high temperature, which leads to production of gases. Gas density profile shows that the gas accumulates on the left side of the domain. But, net mass of gas close to left end depends both on void fraction and density, and void fraction is very low close to the left end, since there's no pyrolysis currently at this location. We get information that the pyrolysis is between x = 0.6 cm and 1.0 cm.

C. Loosely coupled approach for Ablation problem with Galerkin FEM

Since, the solution had convergence issues due presence of oscillations upon including the terms, which were neglected in above simplification, we tried to solve two sets of equations, i.e. (1), (4) and (2), (3) separately in a loosely coupled fashion, in which the in-house finite element based code, MIG was modified to solve given sets of equations in a loosely coupled manner in a generic way. The advantages of this approach lies in being able to selectively identify the root cause of problem of convergence issue and also in solving different equations sets in their respective time scales. The modified code was then tested for given set of Euler equations, to test its running, and results showed were very close to earlier obtained results. See figure 7 for comparison. This helped us in identifying the root cause of problem in the gas equations, and then the focus was shifted to solving Gas equations, (i.e. equations, (2) and (3)) separately given a temperature and resin density profile.

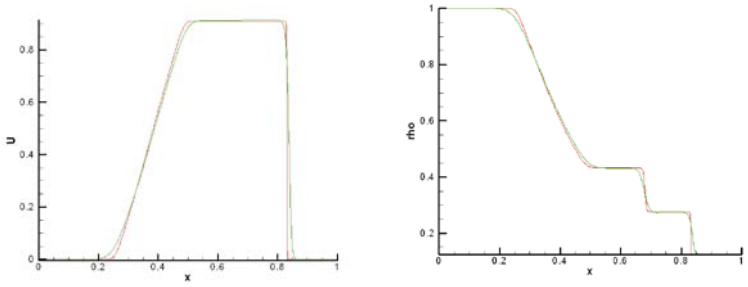

Fig. 7: Solution obtained for Euler equations by modifying MIG into solving separate sets of equations in loosely coupled fashion. Red solution shows, Euler equations solved all together, and green solution shows Euler equations solved in loosely coupled fashion.

We also tried solving Euler equations in a smaller domain and with higher pressure gradients in the solution, since actual problem faces higher pressure gradients in smaller domain, and this becomes more challenging due to high velocities that are generated in the solution, which means stronger oscillations, and this brings in difficulties of convergence issues which were faced. Figures (8 – 10) below, shows some of the results with Euler equations in a domain size of 1 cm, and higher pressure gradients. First result (Figure 8) is comparison of Euler equations solution with all boundary conditions as applied in earlier problems, but smaller domain. A stronger diffusion was required to lead to convergence, and shown solution appears little diffused, because the characteristics have not yet fully developed. Time-step for this simulation is 1.0e-3 sec, and total run time for the solution is 2.0e-3 sec. The comparison is made with the figure on the left, which shows Euler equations solution (solved on a bigger domain of 1 m, with same boundary conditions). Here also we see the solution characteristic has not yet developed at Δt = 2.0e-3 sec, but both the solutions share same behavior. Another set, was run for lower boundary conditions for density (figure 9) on both ends, since we actually have lower densities of order of 1.0e-02 in the beginning solution. The solution is again compared with the bigger domain's solution and both have reasonable agreement. A third case was run with Pressure values of 1.0e05 Pa and 1.0e03 Pa on left and right sides respectively, with bigger domain, (since this was difficult to converge, the problems will only increase with a smaller domain) and solution is shown in figure 10.

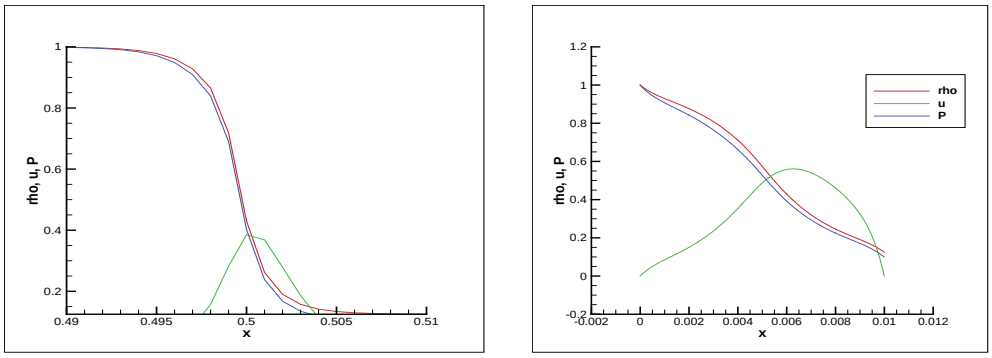

Fig. 8: Comparison of Euler equations solution in a domain of 0.01 m at t = 2.0e-03 sec. Both the above results show quite a good resemblance

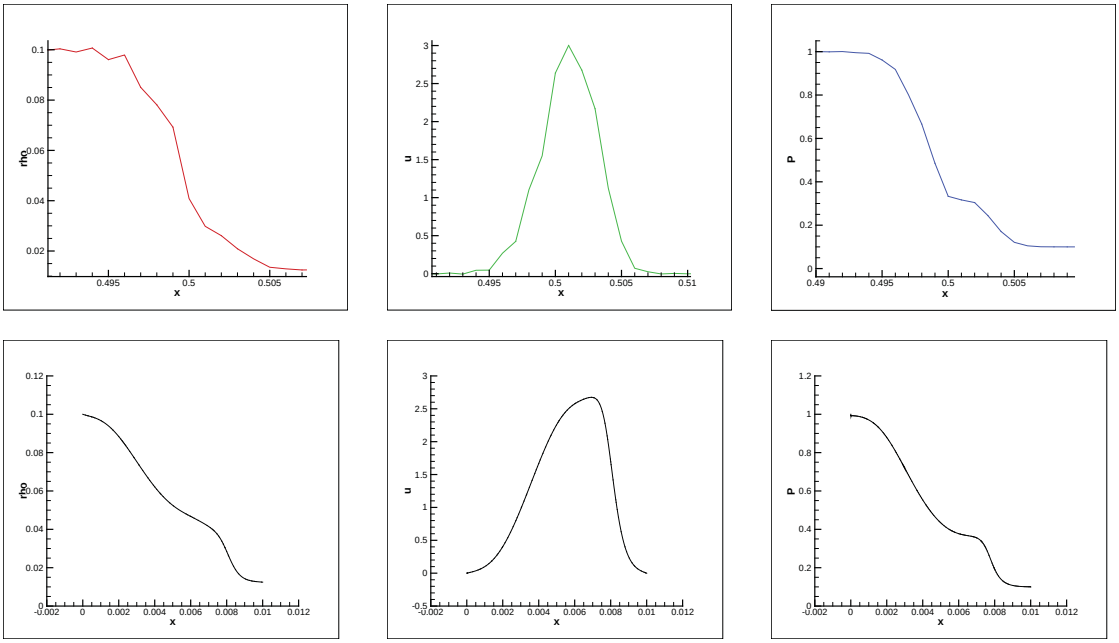

Fig. 9: Comparison of solution of Euler equations with smaller domain and smaller density boundary conditions. Above three plots show, r, u, and P for bigger domain, (of size 1 m), and bottom 3 plots show r, u and P for smaller domain at 7.2e-4 sec. Again we see close resemblance to have some faith on smaller domain solution.

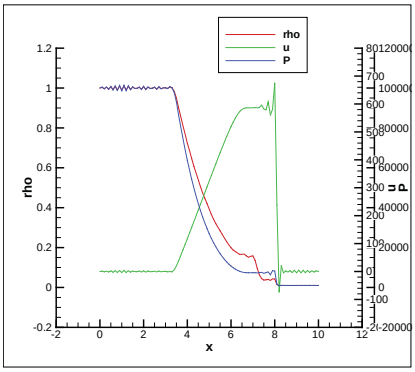

Fig. 10: Above plot shows solution of Euler equations with Pressure boundary conditions, as P = 1.0e05 Pa @ x = 0 m and 1.0e03 @ x = 10.0 m. In spite of using SGM, we still see oscillations in the solution.

After this, a preliminary solution of ablation with all terms in equations (1) – (4) included was attempted with a moderate temperature and density profile as shown. As we cranked up temperature, oscillations became more prominent, and it became difficult to curb them with SGM.

D. Euler equations and Ablation problem with Explicit Runge Kutta Discontinuous Galerkin method

As a very simple test for Explicit Runge Kutta Discontinuous Galerkin method, we verified the case of advection of sine wave, and square wave through the domain $x \in (0,1)$ through a total time of 100 sec. No limiters were used in the simulation, and the obtained results showed it best to use at least k = 2 polynomial order for Legendre polynomials. For lower order solutions were too dissipative. We used Godunov flux only, with Explicit Runge Kutta discontinuous Galerkin scheme.

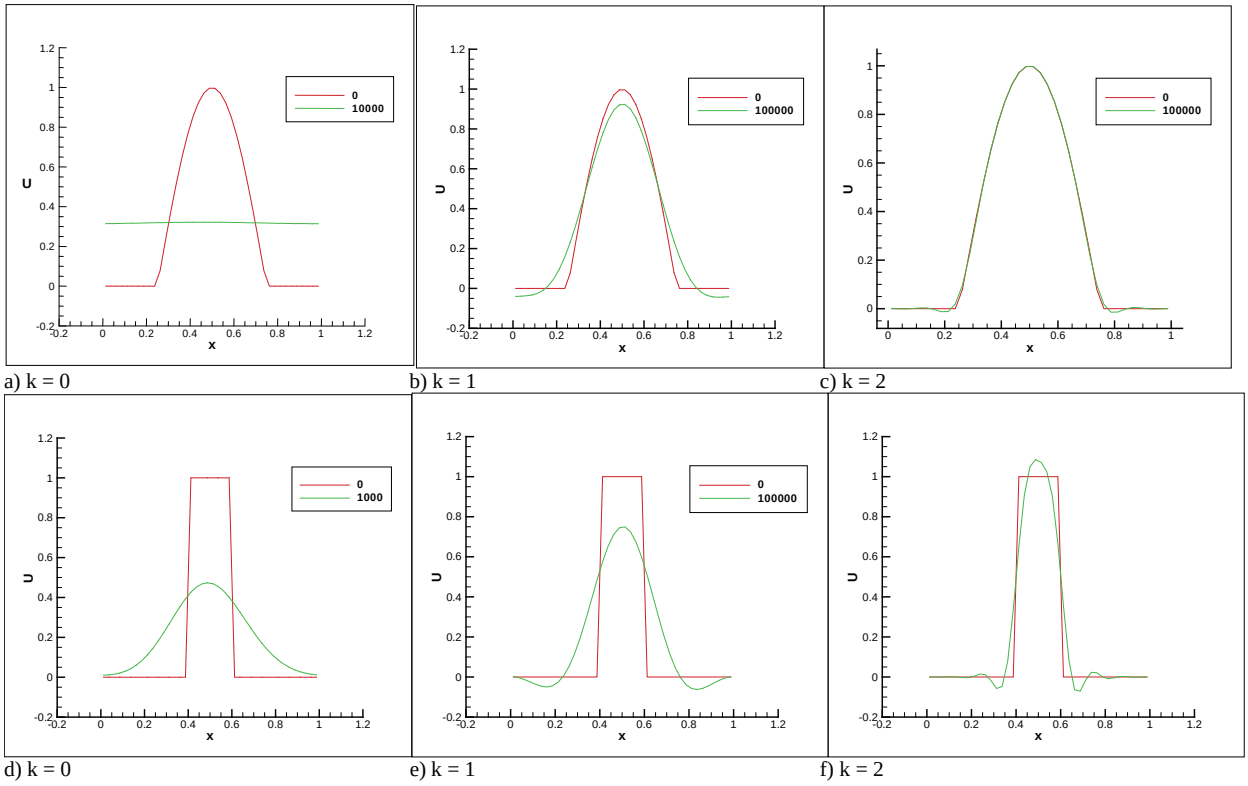

a) k = 0 b) k = 1 c) k = 2

d) k = 0 e) k = 1 f) k = 2

Fig. 11: Advection of a sine wave (a – c) and square wave (e – f), using explicit RKDG method. Green line denotes solution after 100 s, and red line denotes initial solution

Results for Euler equations, for the shock tube problem, are given below,

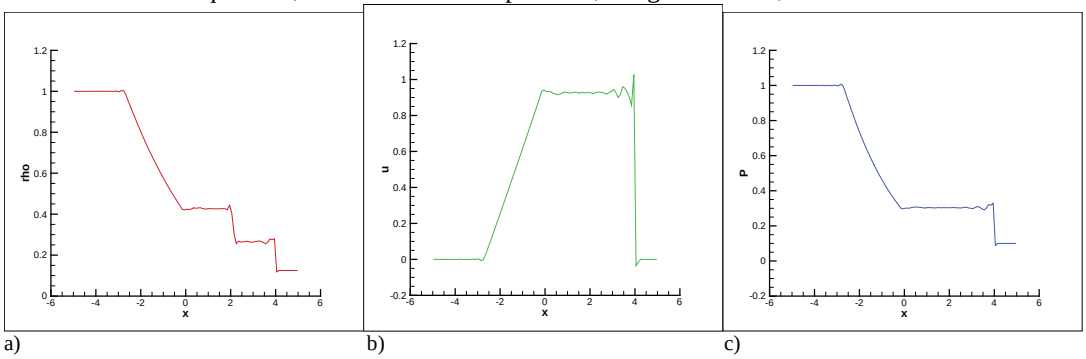

a) b) c)

Fig. 12: Solution for Shock tube problem (Euler equations), using Explicit RKDG method, and Godunov flux. We show density, velocity and pressure profile at t = 2.28 sec

The result is compared with the exact solution. The shock location is predicted to be at 4 m, which is exact solution. There are some oscillations with the shock, but they are never allowed to grow, due to TVD nature of RKDG scheme. The result of Euler equations for Sod's shock tube was compared with that of MIG (using SGM), and we found RKDG to predict correct shock speed as compared to MIG code, which has some error in prediction of shock's speed.

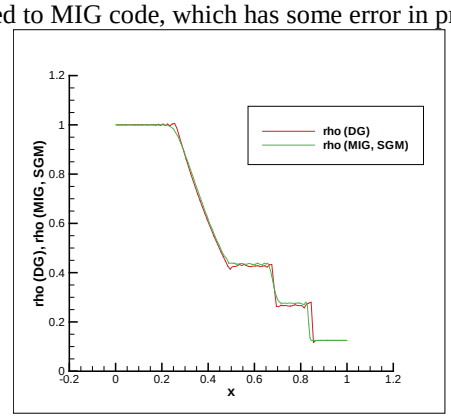

Fig. 13: Density result for shock tube problem compared for explicit RKDG method and Galerkin finite element using SGM. Above result of density is at t = 0.2 sec

We attempted Explicit RKDG code for Ablation problem. Time step for solution was 1.0e-08 sec. Due to pressure at right boundary being fixed at 0.22 atm, and temperature (hence pressure) rising inside the domain, we saw fluctuations in velocity, these fluctuations were strong, and with larger time steps will cause solution to blow up. At this slow time, in the beginning of simulations, no significant pyrolysis is observed, and so all the effect seen is due to thermodynamics of pressure rising with temperature. Below shown is one of simulations, (with pressure boundary condition applied), and total time of 5.14 ms. We see that pyrolysis has hardly begun, from resin density plot. Gas density falls on right end of the domain, and has just begun to increase. Gas velocity being governed by only thermodynamics and not due to gas generation by pyrolysis is up to 4 m/s, and temperature at right end is nearly 790 K. Total number of elements used are 200.

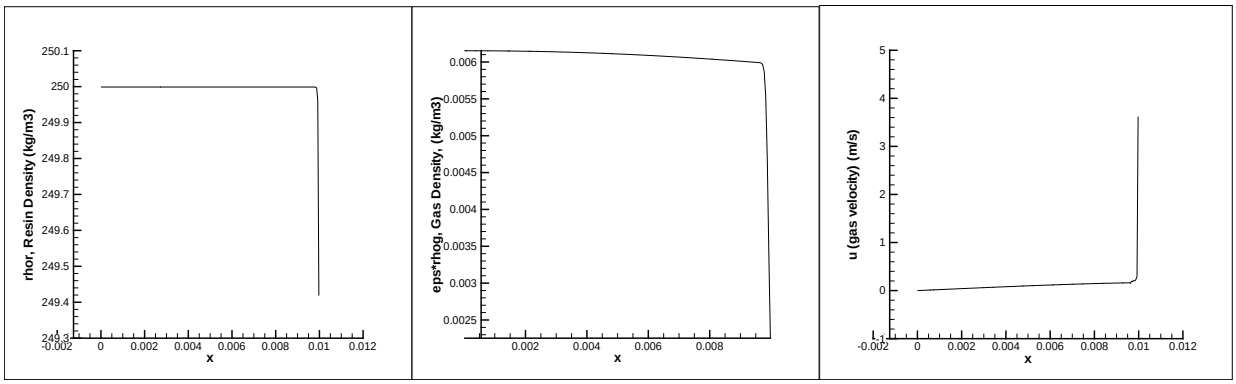

a) b) c)

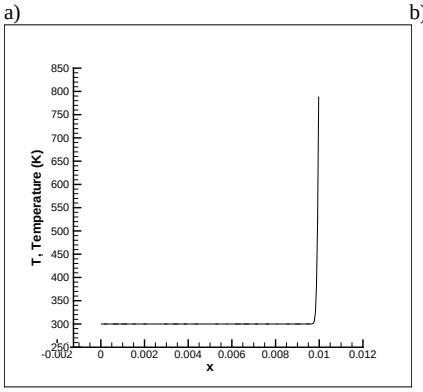

d)

Fig. 14: Thermal Ablation solution with Explicit RKDG method, and total time of 5.14 ms. Pressure at right boundary is fixed at 0.22 atm, that causes high fluctuations in velocity, and causes simulation eventually to blow up.

Another simulation with no pressure boundary condition on right end of domain, and with only 20 elements, run with time step of 1.0e-08 sec, and up till total time of 17 ms. Gas velocity goes to a maximum of 110 m/s, at around 8.5 ms. Temperature goes to 2085 K at right end of the domain, at 17 ms. In plot of resin density we can also see the pyrolysis region near the right end of the domain. Right end has almost reached to the point of zero resin density, i.e. material has completely charred over there.

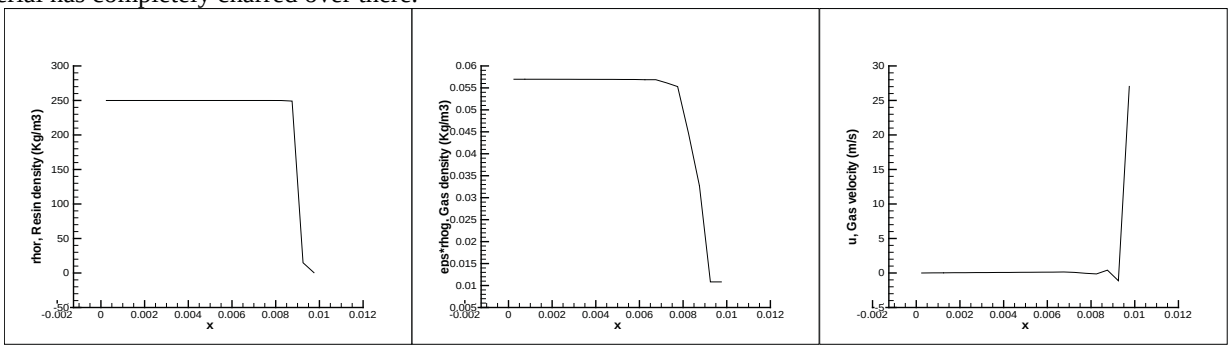

a) b) c)

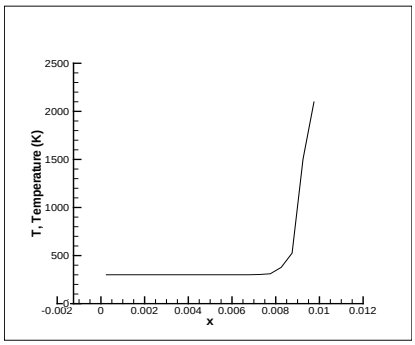

d)

Fig. 15: Simulation for Ablation problem, with no pressure boundary condition at 17 ms (using explicit RKDG method)

Another set of results that were obtained for total time of 56.11 ms. While running animation of results, we see that gas density is undergoing a cycle of increase and decrease, on the left side of domain. Its maximum value inside the domain is 0.18 Kg/m^3. Gas velocity has oscillations in the data by this time. Temperature profile hits a 2281 K at around 20 ms, after which its increase is less compared to before 20 ms.

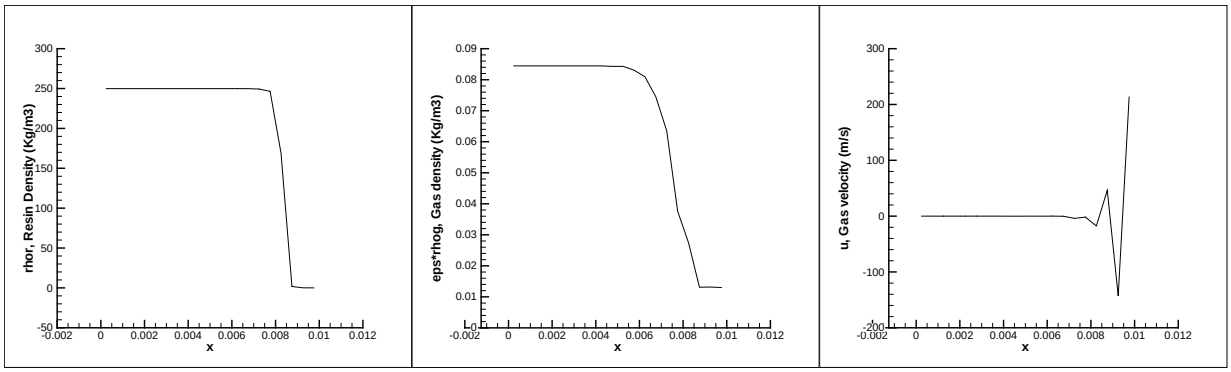

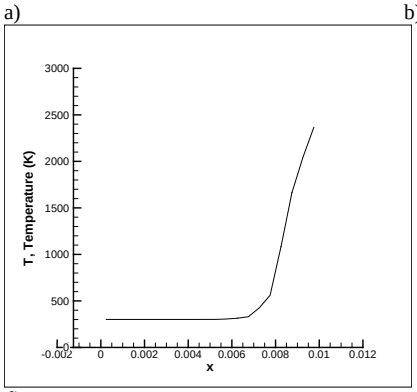

Fig. 16: Solution for thermal ablation problem at 56.11 ms. Solution shows oscillatory behavior in velocity. (Obtained using explicit RKDG)

E. Euler equations and Ablation equations result with Explicit DG method in MIG

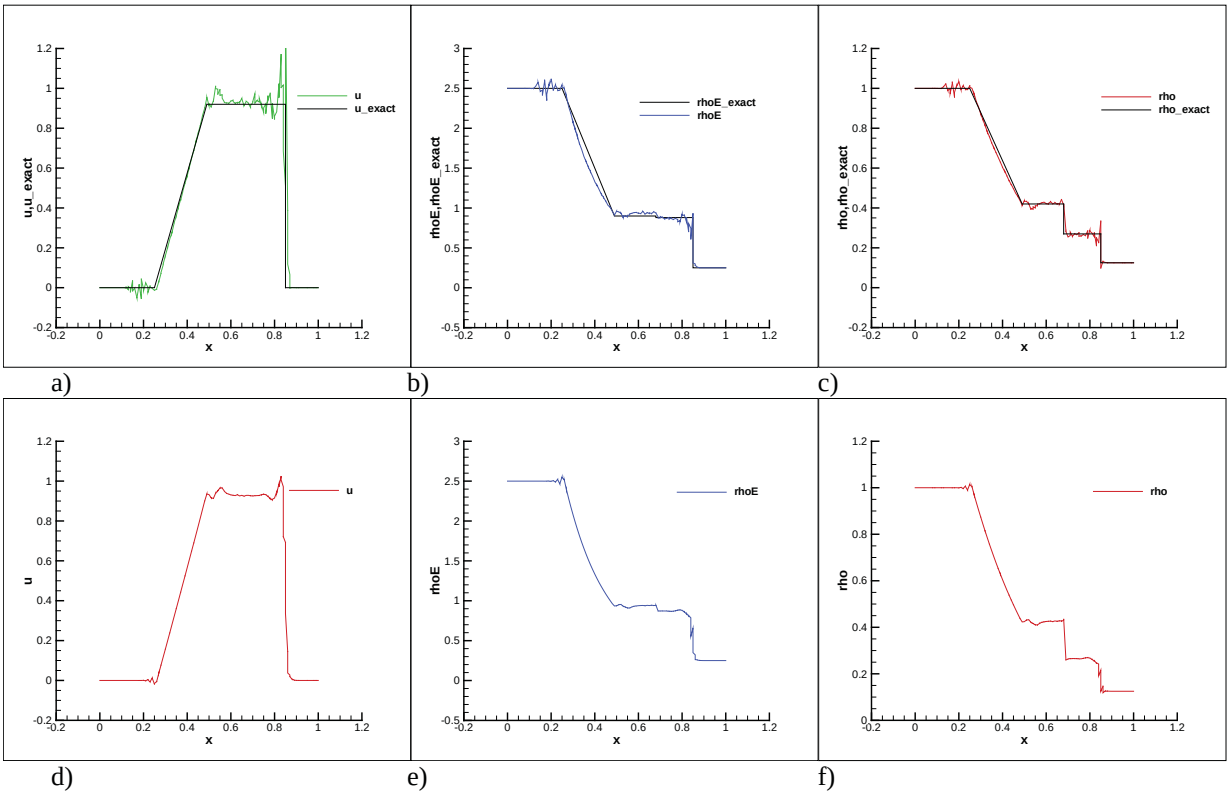

Fig. 17: Results obtained for shock tube problem using Explicit DG method into MIG (using Godunov flux solver, a) – c), and LLF solver d) – f)). Lesser oscillations are observed with LLF. Time step = 1.0e-4 s, total time = 0.2 s

Ablation problem was attempted with Explicit DG method using LLF, and similar issues of velocity fluctuations were faced with this case. Given below are results obtained at time of 0.25 ms. At this early stage pyrolysis has not begun significantly, therefore resin density is nearly constant throughout the domain.

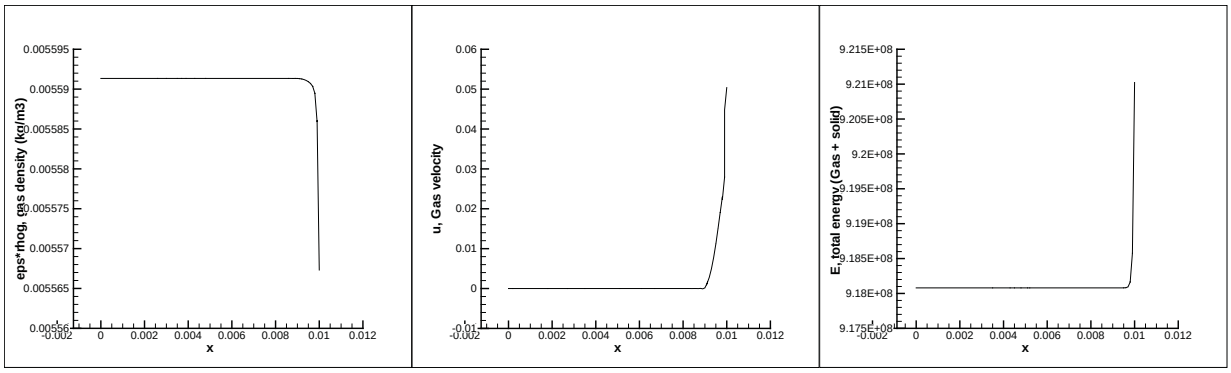

a) b) c)

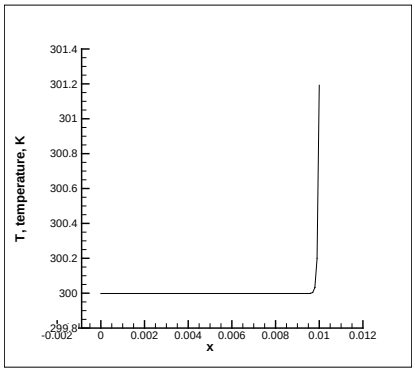

d)

Fig. 18: Results with Explicit DG method for Ablation problem (using LLF), at a total time of 0.25 ms

F. Euler equations and Ablation equations result with Implicit DG formulation in MIG

Here the role of Jacobian is very crucial and as seen, only LLF worked to solve for Euler equations. There's a Jacobian linearization check that should be verified prior to use of the Jacobian, for good convergence. Results obtained with Euler equations are as follows. As compared with explicit DG cases, we see the oscillations in the solution are suppressed due to additional artificial dissipation due to time integration scheme. Higher the time step for integration, more the dissipation of oscillations. Coupling of jacobians from adjacent elements is also crucial, for good convergence. Results for Euler equations, at time step of 10^{-4} s, and a total time of 0.2 s are shown below.

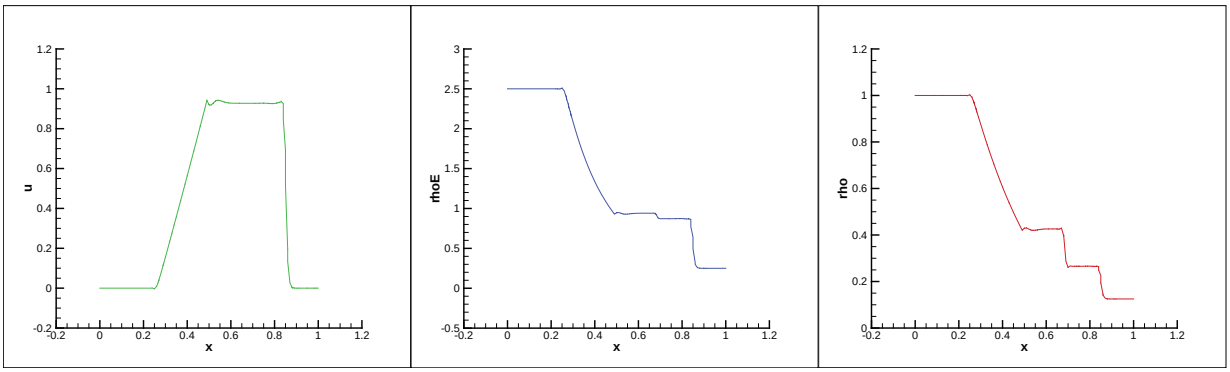

a) b) c)

Fig. 19: Results for Euler equations with Implicit DG method at time step of 10-4 sec, for a total time of 0.2 s. Only Local Lax-Friedrichs flux was successful with Implicit DG

Ablation problem with Implicit DG method took significantly large number of iterations to converge, and have yet to be resolved for their convergence, by working on Jacobians involved in this problem. Below shows results with Implicit DG method at total time of 0.032 ms, run with time step of 1.0e-06 s.

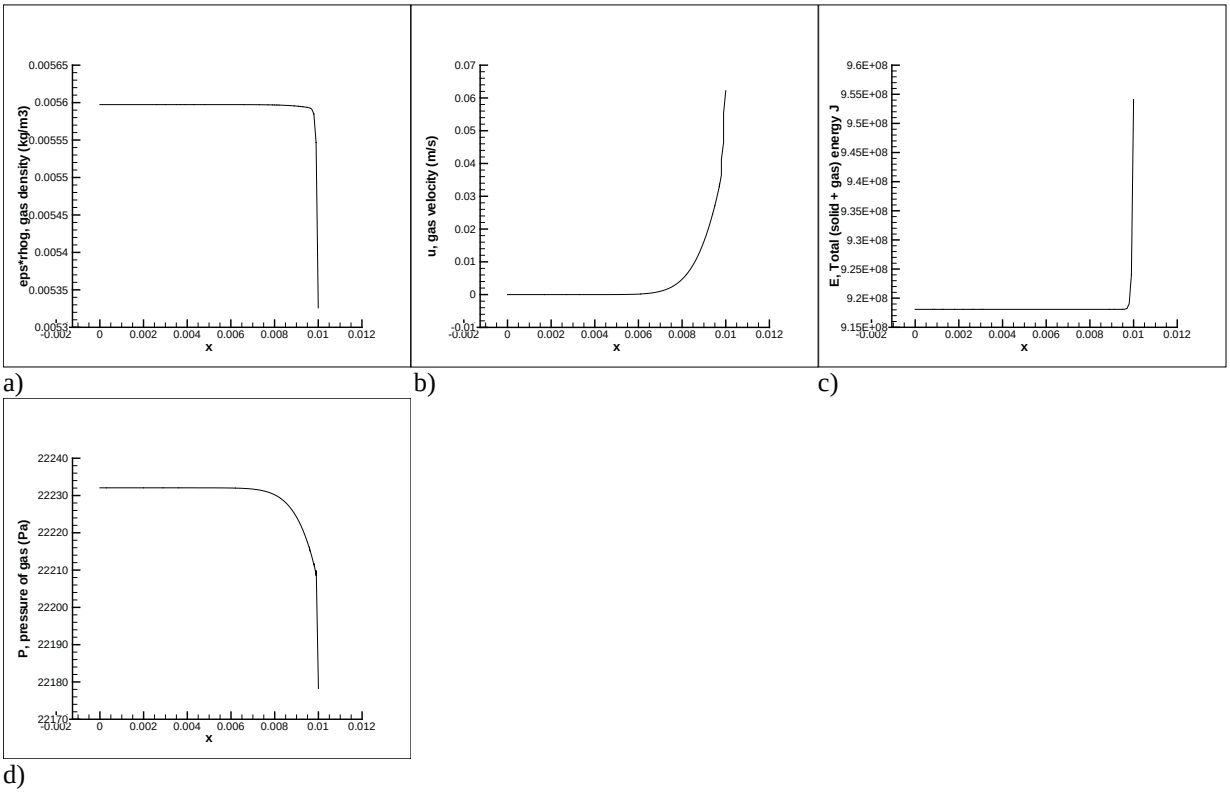

Fig. 20: Result of Ablation problem with Implicit DG method at t = 0.032 ms

VI. Conclusion

Various attempts were made to get solution using Galerkin based Finite element method, using SGM for selective diffusion. But as the pressure gradient that drives the flow increases we see that solution develops oscillations which becomes difficult to curb through use of SGM. This was observed when Euler equations were solved with higher pressure on the boundary conditions. The next step is to try Discontinuous Galerkin based Finite element methods, since they employ approaches similar to flux splitting, which have been successfully used in the area of finite difference and finite volume. Special focus will be on Runge Kutta Discontinuous Galerkin method.

Appendix

Expressions in Matrix of Jacobian of Inviscid Flux

The expressions for A, B, C, D, E and F in matrix are given by,

$$A = \frac{\varepsilon\left(P.C_{pr} + h_r^0 R_{gas}\rho_g\right)}{\left(\rho_c C_{pc} + \rho_r C_{pr} + \varepsilon\rho_g \deg\right)}$$

$$B = -u^2 + \frac{1}{2\rho_g}\frac{\left(\varepsilon u^2 \rho_g^2 R_{gas} + 2P\left(\rho_c C_{pc} + \rho_r C_{pr}\right) - 2\varepsilon\rho_g^2 e_g R_{gas}\right)}{\left(\rho_c C_{pc} + \rho_r C_{pr} + \varepsilon\rho_g \deg\right)}$$

$$C = -u^3 + \frac{u}{2\rho_g}\frac{\left(\varepsilon u^2 \rho_g^2 R_{gas} + 2P\left(\rho_c C_{pc} + \rho_r C_{pr}\right) - 2\varepsilon\rho_g^2 e_g R_{gas}\right)}{\left(\rho_c C_{pc} + \rho_r C_{pr} + \varepsilon\rho_g \deg\right)}$$

$$D = 2u - \frac{\varepsilon\rho_g u R_{gas}}{\left(\rho_c C_{pc} + \rho_r C_{pr} + \varepsilon\rho_g \deg\right)}$$

$$E = e_g + \frac{3}{2}u^2 - \frac{\varepsilon u^2 \rho_g R_{gas}}{\left(\rho_c C_{pc} + \rho_r C_{pr} + \varepsilon\rho_g \deg\right)}$$

$$F = \frac{\varepsilon\rho_g R_{gas}}{\left(\rho_c C_{pc} + \rho_r C_{pr} + \varepsilon\rho_g \deg\right)}$$

Linearization check for a Jacobian used for implicit time integration method

Jacobian formed by a derivative of a flux vector w.r.t. the solution vector, must be verified especially for DG formulation, where we have F+, and F-, which depend on some maximum or absolute value, for Linearization check. The procedure for this is,

1) Introduce a small perturbation δU in U, the solution vector
2) Calculate $F|_{U+\delta U} - F|_U$
3) This should equal $J|_U.\delta U$

A good convergence is usually likely with above criteria met for the implicit method.

Acknowledgement

The authors would like to thank Dr. Ryan Gosse, Research Scientist at AFRL, for his helpful discussions over simulation results of current Ablation problem, and acknowledge Florida center of Advanced Aero-propulsion (FCAAP) and the department of Mechanical & Aerospace Engineering Department at University of Florida, for their partial support.

References

[1]A. Ayasoufi, R. K. Rahmani, G. Cheng, R. Koomullil, K. Neroorkar, "Numerical Simulation of Ablation for Reentry Vehicles", *9th AIAA/ASME Joint Thermophysics and Heat Transfer Conference*, AIAA 2006-290838, 5-8 June 2006.

[2]M. J. Wright, D. Bose, J. Olejniczak, "Impact of Flowfield-Radiation Coupling on Aeroheating for Titan Aerocapture", *Journal of Thermophysics and Heat Transfer*, 19(1), January – March 2005.

[3]P. Reynier, "Convective Blockage during Earth Re-entry. A review.", *40th Thermophysics Conference*, AIAA 2008-3806, 23 – 26 June 2008.

[4]R. C. Gosse, "Ablation Modeling of Electro-magnetically Launched Projectile for Access to Space", *Ph.D. Dissertation*, University of Minnesota, October 2007.

[5]R. C. Gosse, G. Candler, ""Ablation Modeling of Electro-magnetic Launched Projectile for Access to Space", *45th AIAA Aerospace Sciences Meeting and Exhibit*, AIAA-2007-1210, 8-11 January, 2007.

[6]H. G. Landau, "Heat Conduction in a Melting Solid", *Quarterly of Applied Mathematics*, 8(1), pp. 81-94, 1950.

[7]L. Roberts, "A Theoretical Study of Stagnation-Point Ablation", *NACA Technical Note 4392*, 1958.

[8]J. E. J. Staggs, "A Simple Model of Polymer Pyrolysis Including Transport of Volatiles", Fire Safety Journal, 34, pp. 69-80, 2000.

[9]R. M. Kendall, R. A. Rindal, E. P. Bartlett, "Thermochemical Ablation", *AIAA 1965-642*, June, 1965.

[10]H. – K. Ahn, C. Park, K. Sawada, "Response of Heatshield Material at Stagnation Point of Pioneer-Venus Probes", *Journal of Thermophysics and Heat Transfer*, 16(3), July – September 2002.

[11]H. – K. Ahn, C. Park, K. Sawada, "Dynamics of Pyrolysis Gas in Charring Materials Ablation", *36th Aerospace Sciences Meeting & Exhibit*, A98-16086, 12 – 15 January, 1998.

[12]G. C. April, "Evaluation of the Energy Transfer in the Char Zone During Ablation", *Ph.D. Dissertation*, Dept. of Chemical Engineering, Louisiana State University, Baton Rouge, LA, May 1969.

[13]R. M. Clever, V. E. Denny, "Response of Charring Ablators to Severe Aerodynamic and Erosion Environments", *Journal of Spacecraft and Rockets*, 12(9), pp. 558-564, 1975.

[14]R. M. Wakefield, W. C. Pitts, "Analysis of the Heat-Shield Experiment on the Pioneer-Venus Entry Probes", AIAA 1980-1494, July 1980.

[15]F. S. Milos, D. J. Rasky, "Review of Numerical Procedures for Computational Surface Thermochemistry", *Journal of Thermophysics and Heat Transfer*, 8(1), Jan. – March 1994.

[16]Y.-K. Chen, W. D. Henline, M. E. Tauber, "Mars Pathfinder Trajectory Based Heating and Ablation Calculations", *Journal of Spacecraft and Rockets*, 32(2), March – April 1995.

[17]Y.-K. Chen, F. S. Milos, D. C. Reda, D. A. Stewart, "Graphite Ablation and Thermal Response Simulation Under Arc-Jet Flow Conditions", *36th AIAA Thermophysics Conference*, AIAA 2003-4042, 23 – 26 June 2003.

[18]Y.-K. Chen, F. S. Milos, "Two-Dimensional Implicit Thermal Response and Ablation Program for Charring Materials", *Journal of Spacecraft and Rockets*, 38(4), July – August 2001.

[19]R. M. Kendall, "An Analysis of the Chemically Reacting Boundary Layer and Charring Ablator. Part V: A General Approach to the Thermochemical Solution of Mixed Equilibrium-Nonequilibrium, Homogenous or Heterogeneous Systems", NASA CR-1064, June 1968.

[20]Anon, "User's manual Aerotherm Chemical Equilibrium Computer Program (ACE 81)", Report UM-81-11/ATD, August 1981.

[21]F. S. Milos and Y.-K. Chen, "Comprehensive model of Mutlicomponent ablation thermochemistry", AIAA 97-0141, Jan 1997.

[22]J. A. Keenan, "Thermo-Chemical Ablation of Heat Shields Under Earth Re-Entry Conditions," *Ph.D. Dissertation*, Dept. of Mechanical and Aerospace Engineering, North Carolina State Univ., Raleigh, NC, 1994.

[23]J. A. Keenan, G. V. Candler, "Simulation of Ablation in Earth Atmospheric Entry," AIAA Paper 93-2789, July 1993.

[24]C. Park, H.-K. Ahn, "Stagnation-Point Heat Transfer Rates for Pioneer-Venus Probes," *Journal of Thermophysics and Heat Transfer*, 13(1), pp. 33–40, 1999.

[25]T. Suzuki, M. Furudate, K. Sawada, "Unified Calculation of Hypersonic Flow field for a Reentry Vehicle," AIAA Paper 2001-0980, Jan 2001.

[26]J. Zhong, T. Ozawa, D. A. Levin, "Modeling of Stardust Reentry Ablation Flows in the Near-Continuum Flight Regime", *AIAA Journal*, 46(10), Oct. 2008.

[27]D. G. Goodwin, CANTERA, Division of Engineering and Applied Science, California Institute of Technology, www.cantera.org.

[28]J. R. Phillips, "Online Curve Fitting and Surface Fitting Web Site", www.zunzun.com.

[29]S. Roy, A. J. Baker, "Nonlinear, Subgrid Embedded Finite-Element Basis for Accurate, Monotone, Steady CFD solutions", *Numerical Heat Transfer, Part B*, 31-135–175, 1997.

[30]C. Hirsch, "Numerical Computation of Internal and External Flows", Vol. 2, *Computational Methods for Inviscid and Viscous Flows*, John Wiley & Sons.

[31]M. Brio, C. C. Wu, "An upwind Differencing Scheme for the Equations of Ideal Magnetohydrodynamics", *Journal of Computational Physics*, 75, pp. 400 – 422, 1988.

[32] http://www.km.kongsberg.com/

[33]W. H. Reed, and T. R. Hill, "Triangular mesh methods for the neutron transport equation", Technical report, *Los Alamos Scientific Laboratory*, 1973.

[34]B. Cockburn, S. Y. Lin and C.-W. Shu, "TVB Runge-Kutta local projection discontinuous Galerkin finite element method for conservation laws III: One dimensional systems", *J. Comput. Phys.*, 84:90-113, 1989.
[35]B. Cockburn and C.-W. Shu, "TVB Runge-Kutta local projection discontinuous Galerkin finite element method for scalar conservation laws II: General framework", *Math. Comput.*, 52:411-435, 1989.
[36]B. Cockburn, S. Hou, and C.-W. Shu, "TVB Runge-Kutta local projection discontinuous Galerkin finite element method for conservation laws IV: The multidimensional case", *Math. Comput.*, 54:545-581, 1990.
[37]B. Cockburn and C.-W. Shu, "TVB Runge-Kutta local projection discontinuous Galerkin finite element method for conservation laws V: Multidimensional systems", *J. Comput. Phys.*, 141:199-224, 1998.
[38]F. Bassi and S. Rebay, "A high order accurate discontinuous finite element method for the numerical solution of compressible Navier-Stokes equation", *J. Comput. Phys.*, 131(2), 1997.
[39]B. Cockburn and C.-W. Shu, "The local discontinuous Galerkin method for time-dependent convection-diffusion systems", *SIAM J. Numer. Anal.*, 35:2440-2463, 1998.
[40]D. N. Arnold, F. Brezzi, B. Cockburn and D. Marini, "Unified analysis of discontinuous Galerkin methods for elliptic problems", *SIAM J. Numer. Anal.*, 39(5):1749-1779, 2001.
[41]C. C. Wang and S. Roy, "Flow shaping using three-dimensional microscale gas discharge", *Applied Physics Letters*, 95, 081501 (2009).
[42]H. Kumar and S. Roy, "Multidimensional hydrodynamic plasma-wall model for collisional plasma discharges with and without magnetic effects", *Physics of Plasmas*, v12, n9, 093508, 2005
[43]B. Cockburn, "Discontinuous Galerkin Methods for Convection-dominated Problems", *Lecture Notes in Computational Science and Engineering*, Vol. 9, High-Order Methods for Computational Physics